Journal of Marine Science and Technology, Vol. 25, No. 6, pp. 640-648 (2017)
DOI: 10.6119/JMST-017-1226-03

STRENGTH ANALYSIS FOR THE RUDDERS OF POWER-FREE UNDERWATER VEHICLE IN KUROSHIO SUBJECTED TO TYPHOON WAVES

Chuan-Tsung Lee[1], Ray-Yeng Yang[2], Huang Hsing Pan[1], and Li-An Kuo[2]

Key words: current electricity, extreme climate, Kuroshio, rudder, underwater vehicle.

ABSTRACT

In this study, a 1/25 hydraulic model of a power-free vehicle was developed. Typhoon waves and Kuroshio current flow in a wave-current flume ($200 \times 2 \times 2$ m^3) were applied to the model for determining the net flow velocity and mooring forces. Through hydraulic experiments with a wave period of 16 s, wave height of 10 m, and ocean current speed of 1.0 m/s, a net flow velocity of up to 3.81 m/s was measured. The maximum lift and drag forces acting on each rudder were calculated through computational fluid dynamics as -245.6 and 151.6 kN, respectively, when the rudders experienced the interaction of typhoon waves and ocean currents. Finite element analysis revealed that the maximum displacement (14.2 mm) occurred at both sides of the tail end of the front rudder and that the deformation ratio of the rudder was within the permitted deformation range. The mechanical behavior of the rudders remained elastic during operation of the vehicle. Numerical calculations and experimental results indicated that the designed rudders were suitable for use in the Kuroshio current region even in the presence of a typhoon with a 25-year return period.

I. INTRODUCTION

An ocean current with stable flow is one of the several environmentally friendly alternatives for electric power generation. Kuroshio, an ocean current in the north Pacific, has a span of 120-170 km, and 75%-80% of its flow is in the north and northeasterly directions. When Kuroshio passes by the eastern coast of Taiwan, the flow's speed is approximately 0.6-1.2 m/s, potentially providing a flow capacity of $20.7 - 22.1 \times 10^6$ m^3/s (Johns et al., 2001; Hsin et al., 2008). The estimated power reserve of the Kuroshio current near Taiwan is at least 30 GW (Hsu et al., 1999; Johns et al., 2001; Tang, 2010). The total power near eastern Taiwan is 4 GW in winter and 10 GW in summer, depending on monsoons and seasonal variations, and it has an average power of 5.5 GW for several representative cross sections (Chao, 2008; Chen, 2010).

To generate power using the Kuroshio current, high-performance turbine generators suitable for flow velocities of less than 1.5 m/s have been built and tested (Pan et al., 2013). To install a dynamo for generating electricity in the area of Kuroshio, a floating vehicle that sinks while the turbine generators are operational and floats while the generators are dysfunctional is required. Any underwater vehicle to be used for this purpose should be power-free because it will be operated far away from the land. However, a power-free vehicle requires an anchor cable set to bear the drag forces and thus prevent the vehicle from being driven by the current.

Unlike airplanes and ships, an underwater vehicle working in the Kuroshio current does not require propellers or jet engines, which provide high velocity over the rudders, thereby increasing the uplifting, descending, or turning power (Felli and Falchi, 2011). A power-free underwater vehicle designed to carry turbine generators and navigate upward and downward in flow of velocity 0.6-0.7 m/s was successfully developed (Pan et al., 2012), and the elastic behavior of the rudders in this vehicle was also reported (Lee et al., 2013).

Although the Kuroshio current is slow, with a maximum velocity of 1.5 m/s, there is a > 80% probability of typhoons passing through the Kuroshio region near Taiwan (Wu and Kuo, 1999; Morimoto et al., 2009; CWB, 2016), which can cause extreme changes in the wave field of the Kuroshio current (Zhou et al., 2008; Lao, 2011). Extreme typhoon waves in addition to the Kuroshio current can result in waves with high amplitudes and periods that might endanger power-free vehicles and seawater turbine generators. During typhoons, a power-free vehicle should submerge; damage is then prevented by controlling the attack angle of its rudders. For power-free underwater vehicles designed to carry turbine generators for the generation of power using the Kuroshio current, the rudders should have sufficient material strength to withstand the accidental impact of ocean

Paper submitted 06/14/17; revised 08/16/17; accepted 12/13/17. Author for correspondence: Huang Hsing Pan (e-mail: pam@kuas.edu.tw).
[1] Department of Civil Engineering, Kaohsiung University of Applied Sciences, Kaohsiung, Taiwan, R.O.C.
[2] Tainan Hydraulics Laboratory, National Cheng Kung University, Tainan , Taiwan, R.O.C.

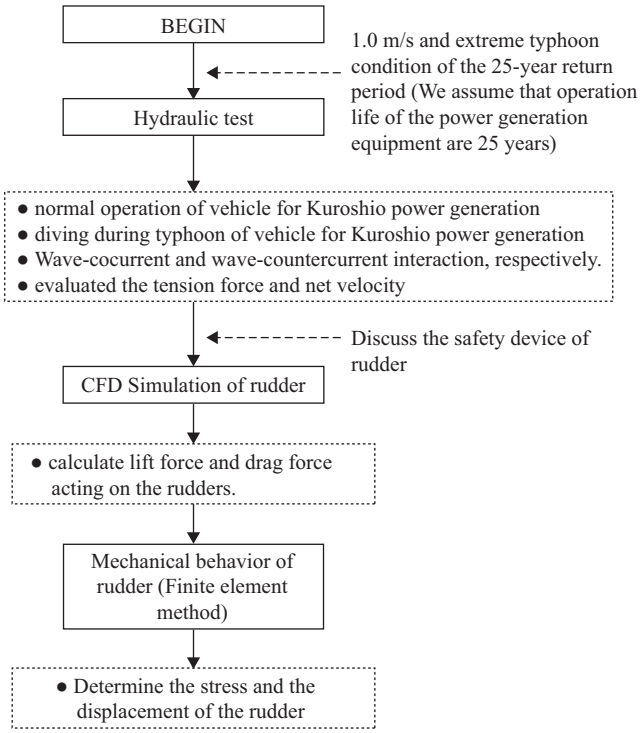

Fig. 1. Main steps in the analysis.

currents induced by typhoons or tsunamis. This study investigated a power-free underwater vehicle for use under extreme wave conditions caused by the interaction of typhoon waves and the Kuroshio current.

The main steps employed to analyze the mechanical behavior of the rudders installed on the power-free underwater vehicle are shown in Fig. 1. The mooring line force and net flow velocity induced by a Kuroshio current of speed 1.0 m/s and an extreme typhoon with a 25-year return period were measured using hydraulic experiments. Furthermore, the lift and drag forces on rudders subjected to the interaction of typhoon waves and the Kuroshio current were calculated using a computational fluid dynamics (CFD) simulation; each rudder's mechanical behavior was determined through finite element calculations.

II. MOORING TRACTION

The developed power-free underwater vehicle with seawater turbine generators was 22 m in length and 8 m in width and moored using a system of cables with anchors, as illustrated in Fig. 2. The vehicle comprised two rudders and several turbine generators and was designed to navigate upward and downward underwater by varying the angle of attack of the rudders.

To determine the net velocity of the current induced by the interaction between extreme typhoon waves and the Kuroshio current acting on the underwater vehicle, a 1/25 hydraulic model test (Fig. 3) was conducted at Tainan Hydraulics Laboratory of Cheng Kung University. According to the similarity of the Froude numbers, the scales of the flow speed and force were 1/5 and 1/15,625, respectively.

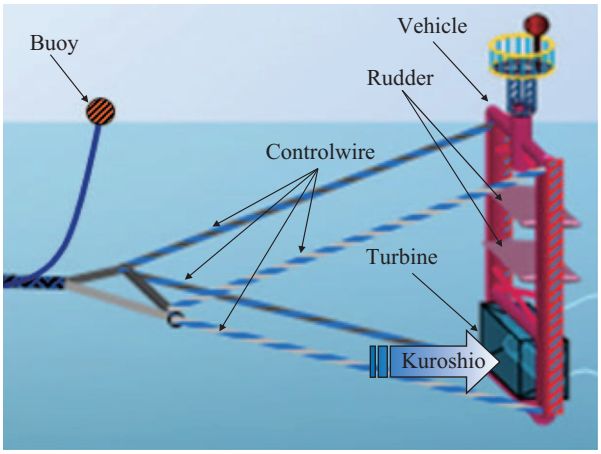

Fig. 2. Schematic of the Kuroshio current power generation system designed by Wanchi Steel Industrial Co. Ltd. (Taiwan).

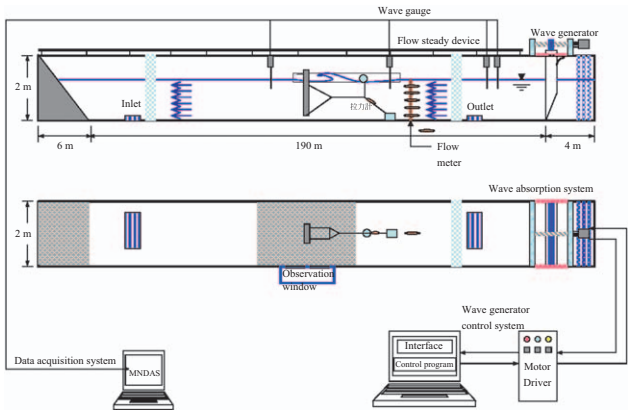

Fig. 3. Configuration of wave-current flume used in the hydraulic model test.

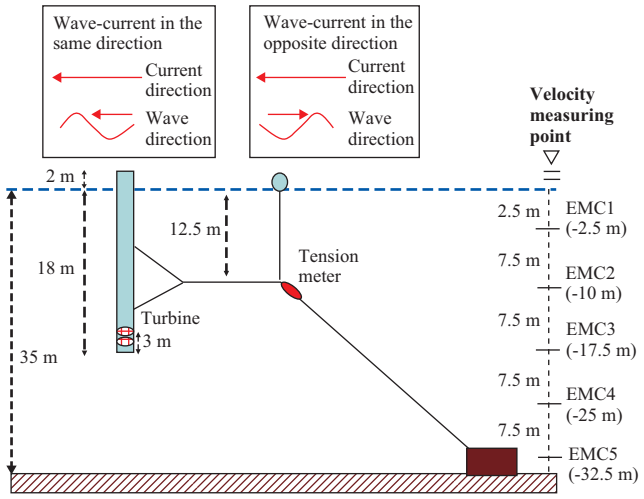

Fig. 4(a). Kuroshio power generation model test for normal operation.

Two types of operation were considered in the hydraulic model test. Fig. 4(a) illustrates the normal operation mode of the vehicle under waves and a current moving in the same and op-

Table 1. Tension force and net velocity of wave-cocurrent interaction (normal operation).

Wave condition (Flow velocity: 1.0 m/sec)							
		(H = 2.5 m, T = 16sec)		(H = 5 m, T = 16 sec)		(H = 10 m, T = 16 sec)	
Position (depth)	Wave phase	Net flow velocity (m/sec)	Tension (ton)	Net flow velocity (m/sec)	Tension (ton)	Net flow velocity (m/sec)	Tension (ton)
EMC1 (-2.5m)	Crest	2.00	EMC4 was the measuring position of tension meter Crest: 9.81 Trough: 0.49	2.40	EMC4 was the measuring position of tension meter Crest: 21.85 Trough: 0	3.54	EMC4 was the measuring position of tension meter Crest: 43.85 Trough: 0
	Trough	0.55		*		*	
EMC2 (-10m)	Crest	1.80		2.17		3.26	
	Trough	0.58		-0.14		-1.18	
EMC3 (-17.5m)	Crest	1.59		2.16		3.13	
	Trough	0.58		-0.08		-0.81	
EMC4 (-25m)	Crest	1.46		2.12		3.12	
	Trough	0.55		-0.06		-0.80	
EMC5 (-32.5m)	Crest	1.32		1.85		2.87	
	Trough	0.50		-0.06		-0.79	
*We ignored this value because the velocity meter was not submerged and noise was encountered in the crest phase.							

Table 2. Tension force and net velocity of wave-countercurrent interaction (normal operation).

Wave condition (Flow velocity: 1.0 m/sec)							
		(H = 2.5 m, T = 16 sec)		(H = 5 m, T = 16 sec)		(H = 10 m, T = 16 sec)	
Position (depth)	Wave phase	Net flow velocity (m/sec)	Tension (ton)	Net flow velocity (m/sec)	Tension (ton)	Net flow velocity (m/sec)	Tension (ton)
EMC1 (-2.5m)	Crest	0.23	EMC4 was the measuring position of tension meter Crest: 1.23 Trough: 12.8	-0.59	EMC4 was the measuring position of tension meter Crest: 0 Trough: 22.35	-1.91	EMC4 was the measuring position of tension meter Crest: 0 Trough: 44.35
	Trough	1.78		*		*	
EMC2 (-10m)	Crest	0.28		-0.32		-1.7	
	Trough	1.55		2.28		3.29	
EMC3 (-17.5m)	Crest	0.42		-0.2		-1.27	
	Trough	1.53		1.98		3.03	
EMC4 (-25m)	Crest	0.43		-0.09		-1.13	
	Trough	1.53		2.03		3.02	
EMC5 (-32.5m)	Crest	0.42		-0.09		-1.05	
	Trough	1.38		1.99		2.88	
*We ignored this value because the velocity meter was not submerged and noise was encountered in the crest phase.							

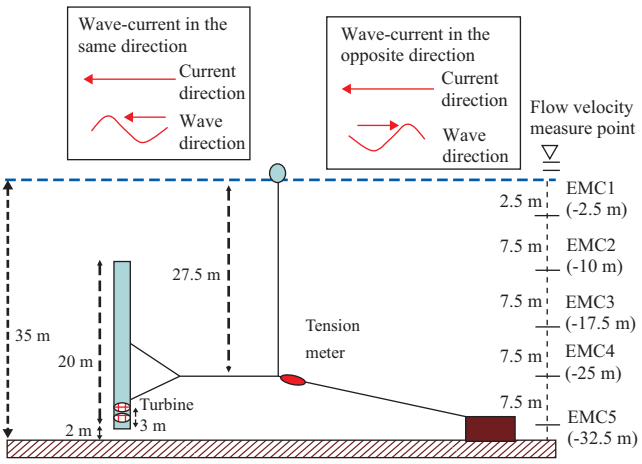

Fig. 4(b). Kuroshio power generation model test for diving operation during a typhoon.

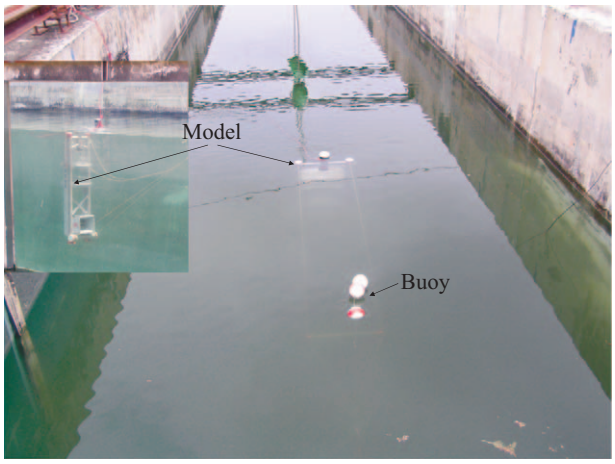

Fig. 5. Experimental setup in the hydraulic model test at Tainan Hydraulics Laboratory.

posite directions. Fig. 4(b) shows operation mode wherein the vehicle dives during a typhoon (diving operation) when subjected to 1.0 m/s ocean current flow and waves caused by an extreme typhoon with a 25-year return period. The operational lifespan

Table 3. Tension force and net velocity of wave-cocurrent interaction (diving operation).

Wave condition (Flow velocity: 1.0 m/sec)							
		(H = 2.5 m, T = 16 sec)		(H = 5 m, T = 16 sec)		(H = 10 m, T = 16 sec)	
Position (depth)	Wave phase	Net flow velocity (m/sec)	Tension (ton)	Net flow velocity (m/sec)	Tension (ton)	Net flow velocity (m/sec)	Tension (ton)
EMC1 (-2.5m)	Crest	2.04	EMC4 was the measuring position of tension meter Crest: 8.26 Trough: 1.49	2.72	EMC4 was the measuring position of tension meter Crest: 15.26 Trough: 0	3.81	EMC4 was the measuring position of tension meter Crest: 33.28 Trough: 0
	Trough	0.61		*		*	
EMC2 (-10m)	Crest	1.81		2.38		3.54	
	Trough	0.63		-0.16		-0.93	
EMC3 (-17.5m)	Crest	1.58		2.07		3.15	
	Trough	0.53		-0.05		-0.79	
EMC4 (-25m)	Crest	1.42		1.92		2.93	
	Trough	0.4		-0.07		-0.81	
EMC5 (-32.5m)	Crest	1.2		1.65		2.63	
	Trough	0.41		-0.08		-0.80	
*We ignored this value because the velocity meter was not submerged and noise was encountered in the crest phase.							

Table 4. Tension force and net velocity of wave-countercurrent interaction (diving operation).

Wave condition (Flow velocity : 1.0m/sec)							
		(H = 2.5 m, T = 16 sec)		(H = 5m, T = 16 sec)		(H = 10 m, T = 16 sec)	
Position (depth)	Wave phase	Net flow velocity (m/sec)	Tension (ton)	Net flow velocity (m/sec)	Tension (ton)	Net flow velocity (m/sec)	Tension (ton)
EMC1 (-2.5m)	Crest	0.37	EMC4 was the measuring position of tension meter Crest: 1.93 Trough: 11.09	-0.55	EMC4 was the measuring position of tension meter Crest: 0 Trough: 21.35	-2.31	EMC4 was the measuring position of tension meter Crest: 0 Trough: 40.34
	Trough	1.93		*		*	
EMC2 (-10m)	Crest	0.45		-0.31		-1.36	
	Trough	1.81		2.35		3.37	
EMC3 (-17.5m)	Crest	0.43		-0.20		-1.28	
	Trough	1.60		2.13		3.24	
EMC4 (-25m)	Crest	0.43		-0.15		-1.18	
	Trough	1.63		2.07		3.21	
EMC5 (-32.5m)	Crest	0.41		-0.14		-1.11	
	Trough	1.36		1.64		2.70	
*We ignored this value because the velocity meter was not submerged and noise was encountered in the crest phase.							

of the power generation equipment is assumed to be 25 years. The wave conditions of a typhoon with a 25 year return period in Taiwan are a wave period (T) of 16 s and a wave height (H) of 10 m. Fig. 5 displays the experimental setup in the hydraulic model test conducted at Tainan Hydraulics Laboratory, where the size of the wave-current flume is approximately 200 × 2 × 2 m^3.

The experimental results of the hydraulic model test for three wave heights H of 2.5, 5.0, and 10.0 m are listed in Tables 1-4. Tension force and net flow velocity were measured at five positions (EMC1-EMC5), as illustrated in Fig. 4. The maximum net flow velocity was discovered to always occur at H = 10 m.

Under normal operation, the maximum net flow velocities for wave-cocurrent interaction, shown in Fig. 6(a), and for wave-countercurrent interaction, shown in Fig. 6(b), were 3.54 and 3.29 m/s, respectively, as given in Tables 1 and 2. The corresponding maximum mooring line tension forces of anchors during the wave-cocurrent and wave-countercurrent interactions were 43.85 and 44.35 ton, respectively (Kuo, 2013). When the power generation system was in the diving position, as shown in Fig. 4(b), the maximum tension mooring forces and net flow velocity for the wave-cocurrent condition were 33.28 ton and 3.81 m/s, respectively (Table 3). For the wave-countercurrent interaction, the maximum tension mooring force was 40.34 ton and the maximum net flow velocity was 3.37 m/s (Table 4). The experimental results indicate that the power-free underwater vehicle always bears smaller tension mooring forces during its diving operation, compared with when it is floating (normal operation). Therefore, to minimize the mooring tractions applied to the power generation system, the vehicle should remain a diving position during typhoons.

According to the results of the hydraulic model test, the maximum net flow velocity under extreme typhoon wave conditions was 3.81 m/s (Table 3), which was 3.81 times the flow velocity

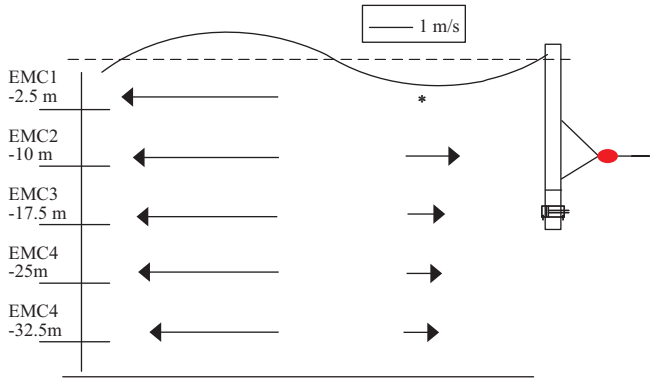

Fig. 6(a). Schematic of net flow velocity of wave-cocurrent interaction (normal operation).

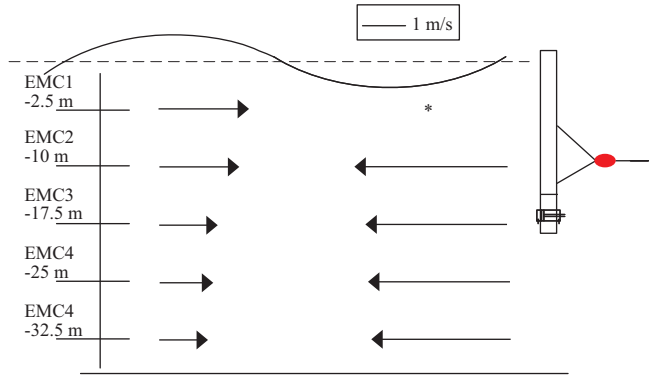

Fig. 6(b). Schematic of the net flow velocity of wave-countercurrent interaction (normal operation).

when no typhoon waves were present (such that the ocean current flow was 1.0 m/s). Thus, the mooring traction acting on the vehicle was $(3.81)^2 = 14.52$ times greater during a typhoon.

In addition, a prototype underwater vehicle with mooring line systems was tested in the Pacific near the southeastern coast of Taiwan in September 2016. The mooring cables broke in the sea test during one of the typhoons. From three data buoys collected by the Central Weather Bureau (Taiwan) (2016), the maximum wave height and wave period during 1999-2016 occurred on September 27, 2016 with $H = 18.7$ m and $T = 15.1$ s; $H = 12.3$ m and $T = 15.5$ s; and $H = 12.47$ m and $T = 11.6$ s at the Su-ao, Guishandao, and Longdong buoys, respectively. The exact dates of the records of the mooring line systems are unavailable.

The maximum wave height and wave period of Su-ao buoy ($H = 18.7$ m and $T = 15.1$ s) were considered for calculating the mooring tractions. The Su-ao buoy was 20 m (-20 m) beneath the sea surface. According to small amplitude wave theory, the particle velocity of the wave in the crest phase is 6.06 m/s if the wave is located at -10 m; for calculations of the particle velocity of a wave, please refer to wave mechanics in any textbook or (Craik, 2004). Assuming that ocean current flow is 1.0 m/s and wave-cocurrent interaction occurs, the net flow velocity is 7.06 m/s. On the basis of hydraulic tests of mooring line systems, Kuo et al. (2013) proposed the following regression formula for estimating the mooring line force:

$$F_r = 4.16V_n^2 + 0.36V_n + 0.24 \quad (1)$$

where F_r denotes the mooring line force (unit: ton) and V_n is the net flow velocity (unit: m/s). The mooring line force for the vehicle at -10 m is 210.1 ton. When the wave height at -20 m is 18.7 m, the particle velocity of the wave in the crest phase is 5.77 m/s, and thus, the net flow velocity is 6.77 m/s. The mooring traction for the vehicle at -20m is 193.3 ton, as calculated using (1). That is, the maximum mooring force increment caused by a net flow velocity of 7.06 m/s is $(7.06)^2 = 49.84$ times that of the ocean current flow. The maximum mooring force in the sea test was three times greater (49.84/14.52 = 3.43) than that simulated and calculated from Tables 1-4. The extreme typhoon conditions that occurred on September 27, 2016, were far beyond the assumption of the hydraulic test; that the typhoon would have a 25-year return period. In practice, the selection of a favorable typhoon return period is required for safely operating underwater vehicles in the Kuroshio current, particularly because of the frequent occurrence of extreme weather.

Unexpected traction on mooring line systems that is caused by typhoon waves can easily damage power generation systems. To reduce the impact of typhoon waves, a power-free vehicle should submerge before the typhoon reaches the Kuroshio power generation area because the maximum flow velocity increments induced by the waves always occur near the sea surface. The Kuroshio power generation vehicle must be steered upward and downward by using its rudder. By varying the angle of attack of the rudders (posture), the position of the power-free vehicle in the Kuroshio current can be changed. Thus, the lift and drag forces acting on the rudders must be estimated from the net flow velocity.

NET CURRENT FLOW ON RUDDERS

From the hydraulic model test, the maximum net flow velocities induced by wave-current interactions and under different conditions were measured to be 3.29, 3.37, 3.54, and 3.81 m/s, as shown in Tables 1-4. The lift force (LF) and drag force (DF) on the rudders depend on the vehicle posture and the wave-current interaction. To keep manufacturing costs low and enable the vehicle to self-float, the rudder must be symmetric and comply with the National Advisory Committee for Aeronautics guidelines, where the span width and chord line length are 4 m and 2.13 m, respectively (Fig. 7). A power-free underwater vehicle with front and rear rudders at the same level was analyzed.

CFD simulations (Miyata et al., 1997; Molland et al., 2007) were conducted to calculate the LF and DF over the rudders due to the net flow velocity. The fluid flow in CFD calculations satisfies the equations of mass conservation and conservation of momentum. The cross-section of the rudder on the x-y plane is shown on the left-hand side of Fig. 7, and the rudder has the shape along the z-axis. Because wave parameters such as the wind direction, wind angle, and wave period are unpredictable

Table 5. Rudder force for extreme typhoon waves and in the Kuroshio current.

	net velocity V_n, (m/s)	C_L	lift force LF, (kN)	C_D	drag force DF, (kN)
front rudder	3.29	-3.373	-138.1	2.084	85.3
	3.37	-3.538	-151.9	2.185	93.8
	3.54	-3.884	-184.1	2.399	113.7
	3.81	-4.474	-245.6	2.762	151.6
rear rudder	3.29	-1.780	-72.9	1.02	41.8
	3.37	-1.865	-80.1	1.069	45.9
	3.54	-2.035	-96.4	1.167	55.3
	3.81	-2.325	-127.6	1.331	73.1
two rudder	3.29	-5.154	-211.0	3.104	127.1
	3.37	-5.404	-232.1	3.255	139.8
	3.54	-5.919	-280.5	3.565	168.9
	3.81	-6.798	-373.2	4.093	224.7

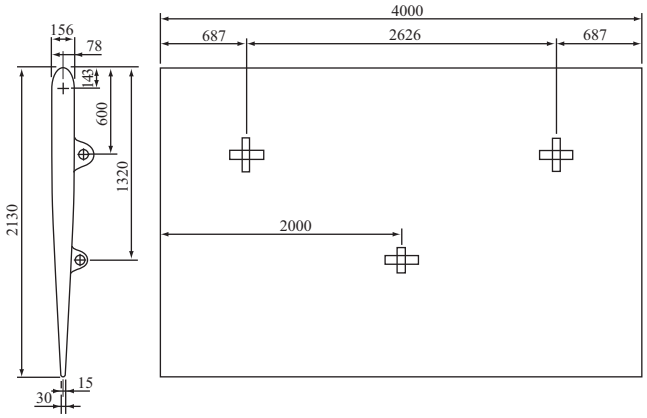

Fig. 7. Schematic of rudder layout and dimensions (mm).

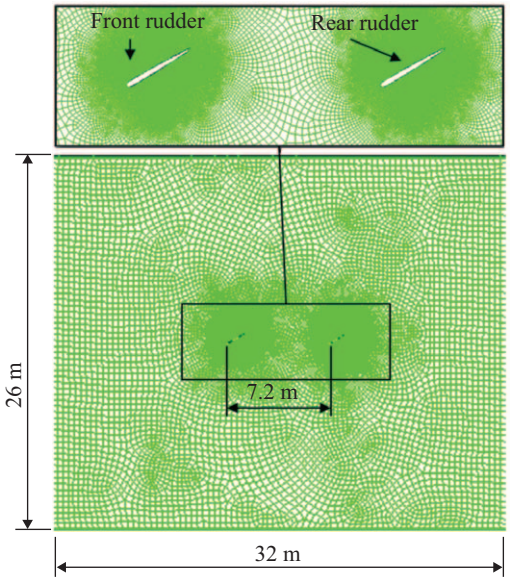

Fig. 8. 2D quadrilateral dominant method control elements and 30° angle of attack.

and complicated in the sea, for simplification, the net flow velocity was substituted for the effect of the wave applied to the rudder in the simulation. The direction of flow in the flow field and that along the z-direction of the rudder were assumed to be constant, and a two-dimensional (2D) CFD study was employed to estimate the LF and DF on the rudders.

Fig. 8 displays the 2D unstructured mesh for two rudders (front and rear) with a distance of 7.2 m, where the computational domain of the flow field is 32 × 26 m^2 and the angle of attack of the rudder is 30°. This angle of attack was selected because this angle results in a high lift and drag coefficient for the power-free underwater vehicle, as reported in (Pan et al., 2012). Denser mesh structures at the leading and trailing edges of the rudder were assigned by using the sizing function shown in Fig. 8, and a triangular element was used in the CFD calculations. The total number of 2D unstructured mesh structures within the computational domain was 83 937 nodes.

Four maximum net velocities-3.29, 3.37, 3.54, and 3.81 m/s-induced by interaction between the Kuroshio current and typhoon waves were used as the inlet flow that causes LF and DF on the rudder, in contrast to (Lee et al., 2013), in which only the Kuroshio current was considered. Both rudders had a symmetrical airfoil shape, as illustrated in Fig. 7.

The LF and DF on the rudders in the computational domain were calculated as follows:

$$\mathrm{LF} = \frac{1}{2} \cdot C_L \cdot \rho \cdot A \cdot V^2 \tag{2}$$

$$\mathrm{DF} = \frac{1}{2} \cdot C_\mathrm{D} \cdot \rho \cdot A \cdot V^2 \tag{3}$$

where C_L and C_D are the lift and drag coefficient, respectively. The parameter A is the projected area of a rudder (m^2), ρ = 1,025 kg/m^3 is the density of seawater, and V represents the average velocity. LF and DF are strongly dependent on the flow velocity.

Table 5 shows the rudder forces calculated using CFD simulation under unsteady state conditions at a 30° angle of at-

tack, where a negative sign indicates a downward pressure. The lift and drag coefficients increased for both the front and rear rudders as the net flow velocity increased. Flow velocity is a dominant factor influencing the LF and DF, as indicated in (2) and (3).

From Lee et al.(2013), the maximum lift coefficient C_L and LF were -1.064 and 4.023 kN, respectively, when the rudders with a 30° angle of attack were submerged in a flow of 1.0 m/s. Compared with flow at 1.0 m/s, the maximum C_L was obtained for the front rudder, equal to -4.474 at 3.81 m/s, resulting in LF = -245.6 kN or an factor increase of 61.04. Typhoon waves can contribute to the net flow velocity, which increases the LF on the rudders, indicating that the vehicle can quickly move upward and downward. Nevertheless, the DF on a rudder at 3.81 m/s was 151.6 kN, which was almost 60.66 times that at 1.0 m/s. The resultant force acting on a rudder was $(-245.6^2 + 151.6^2)^{0.5} = 288.6$ kN for the vehicle in flow with velocity 3.81 m/s. This indicates that more resultants apply to the rudder and power generators, causing more damage to the vehicle. Therefore, vehicles working in the Kuroshio current area should be submerged to reduce the damaging effect of typhoon waves.

The LF and DF acting on the rear rudder, as detailed in Table 5, are always lower than those on the front rudder. This is because the wake induced by the front rudder affects the downstream flow field near the rear rudder. The LF and DF on the rear rudder were discovered to be 52.7% and 48.9% of those of the front rudder for an angle of attack of 30°. This result has crucial design implications for underwater vehicles with front and rear rudders or multiple rudders.

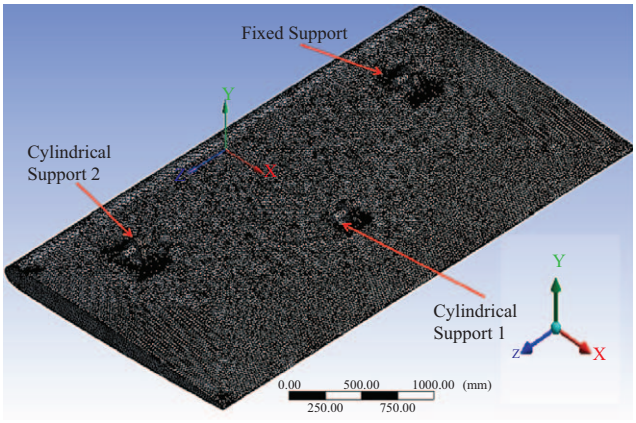

Fig. 9. 3D structured elements of the rudder with three supports.

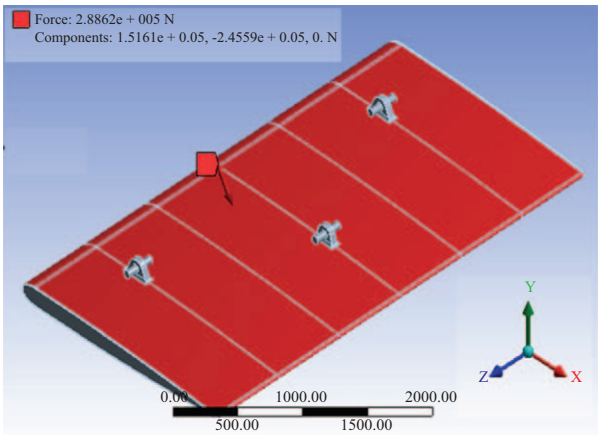

Fig. 10. LF and DF acting on the rudder.

IV. MECHANICAL BEHAVIOR OF THE RUDDERS

The power-free vehicle must be sufficiently strong to resist occasional extreme waves caused by typhoons and other extreme weather in case it cannot submerge quickly enough. Because the front rudder always bears higher LFs and DFs than the rear rudder (Table 5), the maximum LF and DF acting on the front rudder are considered as applied loads during the rudder design. That is, a net flow velocity of 3.81 m/s is considered to determine the mechanical behavior of the rudder. Therefore, the maximum LF and DF of -245.6 and 151.6 kN, respectively, were employed to calculate the stresses and deformations of a rudder by using ANSYS.

The rudder was assumed to be constructed from structural steel having a density of 7.85×10^{-6} kg/mm^3, tensile yield strength of 250 MPa, and tensile ultimate strength of 460 MPa. The rudder was 4 m wide, 2.13 m in chord line length, and 4.5 mm thick. Three supports (two cylindrical supports and one fixed support) were affixed on the rudder in the calculations, as shown in Fig. 9. The fixed support and cylindrical support 2, on both sides of the rudder, were designed to carry the seawater turbine generator and a cylinder. The third support, located at the center of the rudder, was cylindrical support 1. Cylindrical supports provide hydraulic power for controlling the angle of attack of the rudder during operation.

A DF of 151.6 kN and LF of -245.6 kN along the x-axis and y-axis (Fig. 10) were applied to the surface of the rudder. It was assumed that no loads acted on the rudder along the z-axis; the resultant force was calculated as 288.6 kN for an angle of -58.3°. This concentrated load was automatically converted into a uniform load during ANSYS calculations to determine the mechanical behavior of the rudder.

The rudder (computational domain) was subdivided into small control elements using three-dimensional (3D) automatic control grids with quartic elements. The relevance valve was 100, sizing relevance center setting was "Fine," and sizing smoothing was "High." Fig. 9 displays the 3D structured elements of the rudder. The mesh structure comprised 498 769 nodes and 260 378 elements.

The distribution of average equivalent (von Mises) stresses on the rudder, according to ANSYS calculations, is presented in Fig. 11. The high equivalent stresses, which are marked in red and orange, are discontinuously distributed on the rudder surface. These peak stresses (218.75-574.88 MPa) can be eliminated by using welding and grinding during the manufacturing process. However, the average equivalent stresses (indicated

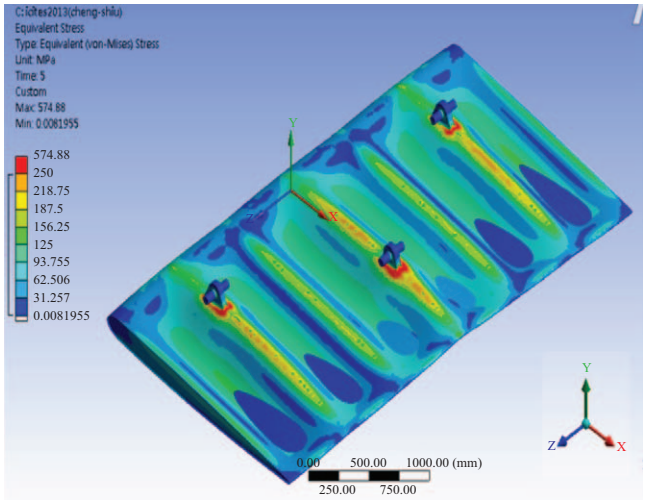

Fig. 11. Equivalent stress of the rudder.

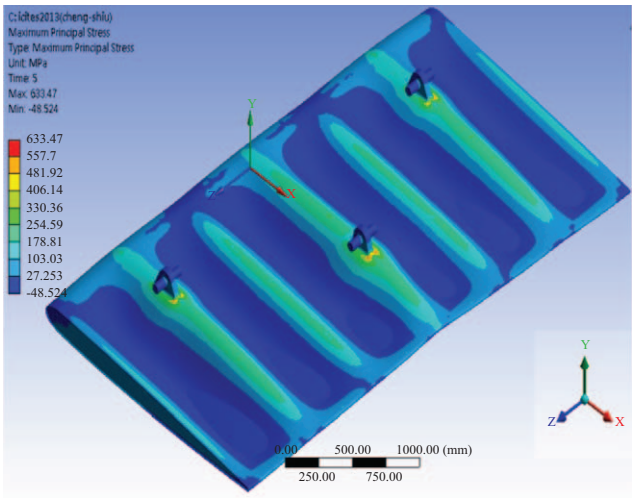

Fig. 12. Maximum principal stress of the rudder.

by yellow) distributed along the *x*-axis are significant, having a maximum value of 218.75 MPa. This von Mises stress is 87.5% of the tensile yield strength. The behavior of the rudder is elastic because the von Mises effective stress is less than the yield stress. In addition, the equivalent stresses (indicated by blue and light-blue) near the tail end of the rudder are not high (< 100 MPa), corresponding to the reduction of the cross-sectional area near the tail end, as illustrated in Fig. 7.

Fig. 12 displays the maximum principal stress of the rudder. Similar to for the equivalent stress (Fig. 11), the maximum principal stresses (red and orange) will be negligible if the rudder is treated through welding or grinding. In this case, the maximum principal stress is 406.14 MPa, 88% of the tensile ultimate strength of the material. Because the underwater vehicle is subject to interaction between typhoon waves and the Kuroshio current, which corresponds to short-term and discontinuous loading (wave period of 16 s), the rudder can bear a maximum principal stress of 406.14 MPa without failure.

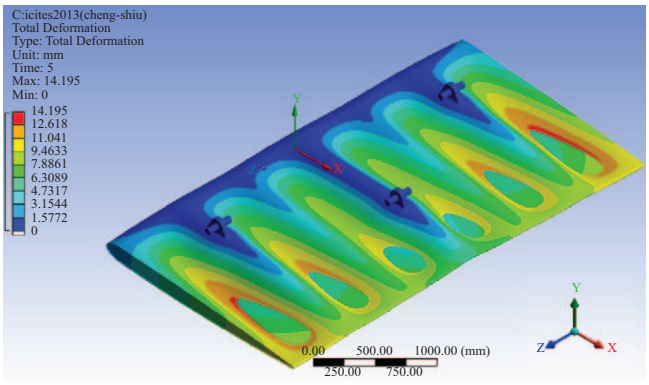

Fig. 13. Total deformation of the rudder.

The total displacements of the rudder were evaluated to consider the rigidity of the rudder's material and are illustrated in Fig. 13. The maximum displacements (14.195 mm) occurred at both sides of the tail end of the rudder (red color). Because the length of the rudder was 4000 mm, the deformation ratio was determined as approximately 1/281. This deformation ratio satisfies the permitted deformation of 1/200-1/800. The locations of these maximum deformations should be reinforced by stiffening the plate, even though the rudder's deformation ratio is within acceptable limits.

V. CONCLUSION

Using hydraulic tests and CFD and ANSYS simulations, the mechanical behavior of rudders on a power-free underwater vehicle subjected to the interaction of extreme typhoon waves and the Kuroshio current was investigated. For a Kuroshio current of 1.0 m/s and extreme typhoons with a 25-year return period, we conclude the following:

1. The maximum tension force in the anchor cable used to moor the power-free vehicle for wave-cocurrent interaction and wave-countercurrent interaction under normal operation was 43.85 and 44.35 ton, respectively.
2. The maximum net current flow applied to the vehicle was 3.81 m/s under normal operation. The mooring traction increased to 14.52 times that with no occurrence of typhoon waves.
3. CFD simulations indicated that net flow velocity is a principal factor affecting the lift and drag coefficients.
4. Although increasing the net flow velocity increased the LF on a rudder, the DF at 3.81 m/s was 60.66 times that at 1.0 m/s for a 30° angle of attack.
5. When the total force (maximum LF + DF) acts on a rudder, the maximum von Mises stress of that rudder is 87.5% of the yield stress; thus, the rudder is operated in its elastic range, and the vehicle can be reliably loaded in the Kuroshio current region.
6. The designed rudder is suitable for Kuroshio current power generation without failure because the maximum principal

stress of the rudder, as calculated using ANSYS, is lower than the ultimate strength of the material.
7. The maximum deformation ratio of the rudder was discovered to be approximately 1/281, which is in the permitted deformation range.
8. To reduce the impact of typhoon waves, the power-free vehicle should be submerged before a typhoon arrives.

ACKNOWLEDGMENTS

The author would like to thank the Ministry of Science and Technology (Taiwan) for financially supporting this research under grant MOST 104-2221-E-151-042 and Tainan Hydraulics Laboratory (Cheng Kung University) for their experimental assistance.

REFERENCES

Central Weather Bureau (2016). http://www.cwb.gov.tw/V7/climate/marine_stat/wave.htm. (in Chinese).

Central Weather Bureau (2016). http://www.cwb.gov.tw/V7/knowledge/planning/index.htm#eq04 (in Chinese).

Chao, S. Y. (2008) Exploring Kuroshio's energetic cores with an ocean nowcast/forecast system. private communication.

Chen, F. (2010). Kuroshio power plant development plan,. Renewable and Sustainable Energy Rev. 14, 2655-2668.

Craik, A. D. D. (2004). The origins of water wave theory. Annu. Rev. Fluid Mech. 36, 1-28.

Felli, M. and M. Falchi (2011). Propeller tip and hub vortex dynamics in the interaction with a rudder. Experiments in Fluids 51, 1385-1402.

Hsin, Y. C., C. R. Wu and P. T. Shaw (2008). Spatial and temporal variations of the Kuroshio east of Taiwan,1982-2005: A numerical study. Journal of Geophysical Research 113, C04002.

Hsu, G, C. T. Liu, C. S. Liu and M. K. Hsu (1999). Power generation from Kuroshio east of Taiwan. Tai Power Engineering Monthly Digest 624, 81.

Johns, W. E., T. N. Lee, D. Zhang, R. Zantopp, C. T. Liu and Y. Yang (2001). The Kuroshio east of Taiwan, moored transport observations from the WOCE PCM-1 Array. Journal of Physical Oceanography 31, 1031-1053.

Kuo, L. A., C. W. Su, H. H. Chen, W. P. Jiang, P. C. Chang, R. Y. Yang, C. Y. Pai and Y. Y. Chen (2013). The tension force test for ocean current power system and encounter probability analysis to the net opposite current. Proceeding of the 35th Ocean Engineering Conference in Taiwan, Kaohsiung, Taiwan, November 21-22, 293-298.

Lao, Y. H. (2011). The head-wind Kuroshio southeast of Taiwan during typhoon Morakot. Master thesis, Institute of Oceanography, Taiwan University.

Lee, C. T., H. H. Pan, R. Y. Yang, P. C. Chang and P. C. Lee (2013). Attack angle and strength of rudders for power-free underwater vehicle in Kuroshio. Proceedings of the Twenty-third International Offshore and Polar Engineering, Anchorage, Alaska, USA, June 30-July 5, 356-361.

Miyata, H., H. Akimoto and F. Hiroshima (1997). CFD performance prediction simulation for hull-form design of sailing boats. Journal of Marine Science and Technology 2, 257-267.

Molland, A. F. and S. R. Turnock (2007). Marine rudders and control surfaces. Butterworth-Heinemann, Elsevier, 2007.

Morimoto, A., S. Kojima, S. Jan and D. Takahashi (2009). Movement of the Kuroshio axis to the northeast shelf of Taiwan during typhoon events. Estuarine, Coastal and Shelf Science 82, 547-552.

Pan, H. H., P. C. Lee, C. T. Lee and P. S. Lin (2013). New waterwheel blades for power generation in Kuroshio. New Developments in Structural Engineering and Construction, edited by S. Yazdani and A. Singh, Research Publishing Services, 1553-1558.

Pan, H. H., P. C. Lee, C. T. Lee and R. Y. Yang. (2012). Rudder controlling of underwater vehicle using in Kuroshio. Advanced Materials Research 512-515, 2662-2669.

Tang, T. Y. (2010). Multi-disciplinary study on the natural resources in the ocean east of Taiwan (I) detailed investigation of current, topography, geology, hydrography and ecology of Lutao area. Report to National Science Council, Taiwan.

Wu, C. C. and Y. H. Kuo (1999). Typhoons affecting Taiwan: current understanding and future challenges. Bull. Amer. Meteor. Soc., 80, 67-80.

Zhou, L. M., A. F. Wang and P. F. Guo (2008). Numerical simulation of sea surface directional wave spectra under typhoon wind forcing. Journal of Hydrodynamics, Ser. B 20 (6), 776-783.